GNSS-Based Orbit Determination for Highly Elliptical Orbit Satellites

Article · January 2009

CITATIONS
3

READS
407

4 authors, including:

Li Qiao
UNSW Sydney
32 PUBLICATIONS **144** CITATIONS
SEE PROFILE

Samsung Lim
UNSW Sydney
251 PUBLICATIONS **1,926** CITATIONS
SEE PROFILE

Chris Rizos
UNSW Sydney
697 PUBLICATIONS **12,997** CITATIONS
SEE PROFILE

GNSS-Based Orbit Determination for Highly Elliptical Orbit Satellites

Li Qiao[1,2*], Samsung Lim[2], Chris Rizos[2] and Jianye Liu[1]

[1]College of Automation Engineering, Nanjing University of Aeronautics and Astronautics, China

(Tel:61-2-93854174, E-mail: l.qiao@student.unsw.edu.a)

[2]School of Surveying and Spatial Information System, University of New South Wales, Australia

Abstract: The Highly Elliptical Orbit (HEO) is useful for a Geostationary/Geosynchronous Transfer Orbit as the orbit can be designed to have a low altitude perigee at the initial orbit and a high altitude apogee at the final orbit of the transfer. Due to the long dwell time at the apogee, however, a study on the feasibility of an autonomous orbit determination for HEO satellites is needed in order to fully take advantage of this. It is envisaged that spaceborne receivers for the current (GPS and Glonass) and upcoming GNSS systems (such as Galileo and Compass) will improve the GNSS-based orbit determination of HEO satellites. This paper investigates the potential of HEO satellite orbit determination using the multi-GNSS constellation, i.e. current 31 GPS satellites, assumed 24 Glonass satellites, planned 30 Galileo satellites and 27 Compass satellites. This paper first reviews the use of pseudorange measurements for orbit determination over the last two decades. Secondly, the paper describes the basic navigation requirements associated with using multi-GNSS in the HEO environment. It is assumed that a multi-GNSS receiver will receive all the signals from all the GNSS systems and utilise pseudorange measurements. The paper presents a navigation algorithm based on a Kalman filter, the state vector of which consists of position and velocity corrections to the nominal reference trajectory and the clock biases. The state vector is then propagated using the orbit and clock dynamics, and updated by the GNSS measurements. The required geometric conditions, precision, update interval and propagation interval are factors to be considered in the design of this algorithm. Test results with simulated multi-GNSS data indicate that the determined orbit remains within an acceptable range, and therefore this algorithm meets the requirement for HEO autonomous satellite navigation.

Keywords: Autonomous navigation, Orbit determination, Extended Kalman filter, Spaceborne GPS, HEO

1. Introduction

Signals from the Global Positioning System (GPS) satellites have been used in many satellite missions. For example, low earth orbit (LEO) satellites can measure GPS signals reflected from the ocean surface for sea state studies. There exist several commercial spaceborne receivers that can provide onboard navigation solutions [1]. The application of the Global Navigation Satellite System (GNSS) for the autonomous navigation of highly eccentric orbit (HEO) satellites has been under consideration for some time. There exist a series of HEO communications and scientific missions under development or proposed for the coming decade [2-5].

The high altitude of a HEO spacecraft presents a very unfavourable environment for the reception of GNSS signals. The most significant difference from the LEO environment is the sparse nature and poor geometric coverage of GNSS signals at high altitudes because the GNSS signal transmitters face towards the nadir, i.e. towards the centre of the Earth. Figure 1 illustrates the geometry when tracking these limb-crossing GNSS signals by a receiver at a higher altitude than that of GNSS. The signals reaching the HEO receiver at this high altitude originate from GNSS satellites on the opposite side of the Earth. If only one GNSS, e.g. GPS, is used, it is difficult to receive four or more satellite signals simultaneously. More importantly, the vehicle dynamics and signals levels are problematic.

Research shows that GNSS signals can be sensed at an altitude exceeding 6,000km, and the side lobe signals can be also tracked [6]. In the case of a HEO antenna fixed to the body, [7] suggested that the HEO antenna towards the nadir at the apogee provides better signal coverage. Nevertheless, GPS-only signals are not plentiful enough.

This paper investigates the feasibility of HEO satellite orbit determination using multi-GNSS systems, i.e. current 31 GPS satellites, assumed 24 Glonass satellites, planned 30 Galileo satellites and 27 Compass satellites [8]. It is assumed that a multi-GNSS receiver will receive all signals from all GNSS systems and utilise the pseudorange measurements. It is assumed that the HEO satellite orbit can be determined within an acceptable range by using main lobe signals only, even if the receiver antenna is not fixed to point in the most favourable direction.

This paper presents a navigation algorithm based on a Kalman filter. The state vector of the equation of the satellite motion consists of position and velocity corrections to the nominal reference trajectory and the clock biases. The state vector is then propagated using the orbit and clock dynamics, and updated by the GNSS

measurements. The simulation results using the expected multi-GNSS signal visibility and navigation accuracy for two mission scenarios are presented.

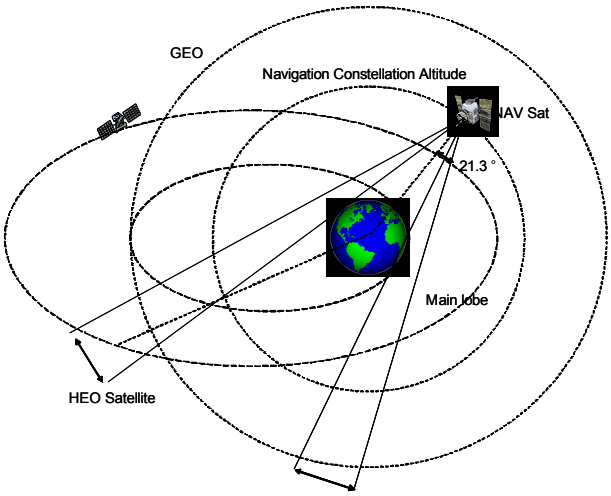

Figure 1. Geometry of GNSS signal reception by a HEO.

2. Orbit Determination Algorithms

2.1 Measurement Models

The observation equation at each epoch is given by:

$$\rho_j = R_j + \delta t_u + v_{\rho j} \tag{1}$$

where

- j GNSS satellite index
- ρ_j pseudorange from the HEO satellite to the navigation satellite S^j
- R_j geometrical distance from the HEO satellite to the navigation satellite S^j
- $v_{\rho j}$ random measurement noise
- δt_u range error equivalent to the receiver clock offset with respect to GNSS time frame

If n satellites are available, the Kalman filter model can be expressed as:

$$Z = h(X) + V \tag{2}$$

where $Z = [\rho_1 \quad \rho_2 \quad \cdots \quad \rho_n]^T$ is the observation vector of pseudorange measurements ρ_j, X is the state vector, $h(X) = [r_1 + \delta t_u \quad r_2 + \delta t_u \quad \cdots \quad r_n + \delta t_u]^T$ is a vector function that defines the relationship between the observation vector and the state vector, and $V = [v_{\rho 1} \quad v_{\rho 2} \quad \cdots \quad v_{\rho n}]^T$ is the receiver noise. Any perturbations not included in *h(X)* are considered to be Gaussian errors with $E[V] = 0$ and $E[VV^T] = R$.

2.2 Dynamic Models

For the deterministic dynamic model of a HEO satellite, the satellite dynamics are utilised to define the equation of motion with respect to the J2000.0 in the Earth Centred Inertial (ECI) coordinate system. The X and Z axes point toward the mean vernal equinox and mean rotation axes of the Earth at January 1, 2000 at 12:00:00.00 UTC respectively. J2000.0 = 2000 January 1.5 = JD 2451545.0 TDT (Terrestrial Dynamical Time).

Assuming that the position vector is $\mathbf{r} = [x \quad y \quad z]^T$ and the velocity vector is $\mathbf{v} = [v_x, v_y, v_z]^T$, the orbit state vector can be written as:

$$\mathbf{X}_{orbit} = \begin{bmatrix} \mathbf{r} \\ \mathbf{v} \end{bmatrix} = [x, y, z, v_x, v_y, v_z]^T \tag{3}$$

In a general form, the equations of motion can be presented as:

$$\dot{\mathbf{X}}_{orbit} = f_{orbit}(\mathbf{X}, t) + \mathbf{W}_{orbit}(t) \tag{4}$$

where f_{orbit} is the function that describes the satellite state dynamics, and $\mathbf{w}_{orbit}(t)$ is the process noise of the state equation. Ignoring the process noise $\mathbf{W}_{orbit}(t)$, the first derivative of the state vector $\mathbf{X}$ therefore is:

$$\dot{\mathbf{X}}_{orbit} = f_{orbit}(\mathbf{X}_{orbit}, t) = \begin{bmatrix} \dot{\mathbf{r}} \\ \dot{\mathbf{v}} \end{bmatrix} = \begin{bmatrix} \mathbf{v} \\ \mathbf{a} \end{bmatrix} \tag{5}$$

where $\mathbf{a}$ is the acceleration of the satellite.

The main component of the satellite acceleration $\mathbf{a}$ depends on the altitude of the satellite orbit. For a HEO satellite whose orbit altitude varies from approximately 3,000km (perigee) to 30,000km (apogee), the acceleration will be perturbed by the two-body attraction, the non-spherical Earth gravitational potential, the luni-solar gravitational potential, etc. Thus, the total acceleration of a HEO satellite can be written as:

$$\mathbf{a} = \mathbf{a}_{Earth} + \mathbf{a}_{Sun} + \mathbf{a}_{Moon} + \mathbf{a}_{\mathbf{w}} \tag{6}$$

where $\mathbf{a}_{Sun}$ and $\mathbf{a}_{Moon}$ are the third-body effects of the Sun and Moon respectively, $\mathbf{a}_{Earth}$ includes the two-body effect and the non-spherical gravitational potential effect from the Earth, and $\mathbf{a}_{\mathbf{w}}$ represents the high-order terms that are considered to be the noise of the system model. Other perturbations (such as atmospheric drag, solar radiation pressure, earth tide, etc.) are assumed to be negligible compared to the remaining effects in $\mathbf{a}_{\mathbf{w}}$.

The main zonal harmonics to be considered are J_2, J_3 and J_4. The non-spherical gravitational potential $\mathbf{a}_{Earth}$ can be represented in the ECI coordinate system as [9]:

$$\mathbf{a}_{Earth} = \begin{bmatrix} -\frac{\mu_e x}{r^3}\left[1 + J_2\left(\frac{R_e}{r}\right)^2 \frac{3}{2}\left(1 - 5\frac{z^2}{r^2}\right) + J_3\left(\frac{R_e}{r}\right)^3 \frac{5}{2}\left(3 - 7\frac{z^2}{r^2}\right)\frac{z}{r} - J_4\left(\frac{R_e}{r}\right)^4 \frac{5}{8}\left(3 - 42\frac{z^2}{r^2} + 63\frac{z^4}{r^4}\right)\right] \\ -\frac{\mu_e y}{r^3}\left[1 + J_2\left(\frac{R_e}{r}\right)^2 \frac{3}{2}\left(1 - 5\frac{z^2}{r^2}\right) + J_3\left(\frac{R_e}{r}\right)^3 \frac{5}{2}\left(3 - 7\frac{z^2}{r^2}\right)\frac{z}{r} - J_4\left(\frac{R_e}{r}\right)^4 \frac{5}{8}\left(3 - 42\frac{z^2}{r^2} + 63\frac{z^4}{r^4}\right)\right] \\ -\frac{\mu_e z}{r^3}\left[1 + J_2\left(\frac{R_e}{r}\right)^2 \frac{3}{2}\left(3 - 5\frac{z^2}{r^2}\right) + J_3\left(\frac{R_e}{r}\right)^3 \frac{5}{2}\left(6 - 7\frac{z^2}{r^2}\right)\frac{z}{r}\right] + \frac{\mu_e}{r^2} J_3\left(\frac{R_e}{r}\right)^2 \frac{3}{2} - J_4\left(\frac{R_e}{r}\right)^4 \frac{5}{8}\left(15 - 70\frac{z^2}{r^2} + 63\frac{z^4}{r^4}\right) \end{bmatrix}$$

where

$r = \sqrt{x^2 + y^2 + z^2}$	distance between the geocentre of the Earth and the HEO satellite
R_e	the Earth mean radius (based onWGS-84 reference frame)
μ_e	the gravitational parameter of the Earth
J_2 J_3 J_4	coefficients are referred to as zonal harmonics, related to the terrestrial model.

The luni-solar gravity force depends on the luni-solar position with regards to the HEO satellite. The luni-solar perturbation is calculated by[10]:

$$\mathbf{a}_{Sun} = \mu_s \left(\frac{\mathbf{r}_s - \mathbf{r}}{\|\mathbf{r}_s - \mathbf{r}\|^3} - \frac{\mathbf{r}_s}{\|\mathbf{r}_s\|^3} \right) \qquad \mathbf{a}_{Moon} = \mu_m \left(\frac{\mathbf{r}_m - \mathbf{r}}{\|\mathbf{r}_m - \mathbf{r}\|^3} - \frac{\mathbf{r}_m}{\|\mathbf{r}_m\|^3} \right)$$

where μ_s and μ_m are the gravitational parameters of the Sun and Moon respectively, and $\mathbf{r}_s = [x_s, y_s, z_s]^T$ and $\mathbf{r}_m = [x_m, y_m, z_m]^T$ are position vectors of the Sun and Moon in the ECI coordinate frame respectively.

The receiver clock is also modelled. The state of the clock deviation X_{clock} is composed of the clock drift and the drift rate, i.e. $\mathbf{x}_{clock} = [\delta t_u \quad \delta t_{ru}]^T$. An exponentially correlated clock model driven by a zero mean white noise is integrated in the process model; referred to as the first order Markov process. For convenience, it is assumed that the four different GNSSs have a common unified time system, and the clock error is:

$$\dot{\boldsymbol{X}}_{clock} = f_{clock}(\boldsymbol{X}_{orbit}, t) + W_{clock} = \begin{bmatrix} \delta t_u & -\frac{1}{T_{ru}} \delta t_{ru} \end{bmatrix}^T + [w_{tu} \quad w_{tu}]^T \qquad (7)$$

The parameter T_{ru} is the clock model correlation time. The resulting state vector is composed of six spacecraft position and velocity components and the receiver clock bias and bias rate. The overall process model can be expressed as:

$$\boldsymbol{X} = f(\boldsymbol{X}) + \boldsymbol{W} \qquad (8)$$

where the state vector $\boldsymbol{X}$, the state model $f(\boldsymbol{X})$ and the measurement noise W, in the ECI frame are given by:

$$\boldsymbol{X} = \begin{bmatrix} \boldsymbol{X}_{orbit} \\ \boldsymbol{X}_{clock} \end{bmatrix}, \; f(\boldsymbol{X}) = \begin{bmatrix} f_{orbit}(\boldsymbol{X}_{orbit}, t) \\ f_{clock}(\boldsymbol{X}_{clock}, t) \end{bmatrix}, \; \boldsymbol{W} = \begin{bmatrix} \boldsymbol{W}_{orbit} \\ \boldsymbol{W}_{clock} \end{bmatrix}.$$

The measurement noise W is expected to have the Gaussian error distribution with $E[\boldsymbol{W}] = 0$ and $E[\boldsymbol{W}\boldsymbol{W}^T] = \boldsymbol{Q}$.

The error covariance matrices $\boldsymbol{Q}$ and $\boldsymbol{R}$ are assumed to be diagonal, which is an important hypothesis when a Kalman filter is used. That is, the perturbations and noises in the process and measurement filter models are uncorrelated.

2.3 The Extended Kalman Filter

A typical navigation solution consists of estimates of spacecraft position, velocity and model parameters of the receiver clock behaviour. In this paper, the estimation is performed using an Extended Kalman Filter (EKF) to to account for the non-linear state dynamics presented in the previous section.

The main advantages of the Kalman filter approach with respect to other algorithms are: 1) it is a statistical filter that provides a reliable accuracy of the solution in the presence of random perturbations; and 2) the implemented dynamic model enables the filter to predict position and velocity vectors at a future time, even in the absence of measurements [11].

The filter measurement model and the system dynamics model are given in Equations (2) and (8). In an EKF implementation, the partial derivative matrices of the predicted state vector rate $f(X)$ and of the predicted measurement vector $h(X)$ at the *k-th* step must be considered:

$$h_k = h(\tilde{X}_k) \qquad H_k = H(\tilde{X}_k) \qquad H = \frac{\partial h(\tilde{X})}{\partial X}$$

$$f_k = f(\tilde{X}_k) \qquad F_k = F(\tilde{X}_k) \qquad F = \frac{\partial f(\hat{X})}{\partial X}$$

where $\hat{X}$ and $\tilde{X}$ are the estimated and the predicted state vectors respectively. From the previous definition, the correction process consists of the following steps [12]:

$$\hat{\mathbf{X}}(k+1/k) = \hat{\mathbf{X}}(k/k) + f[\mathbf{X}(k)] \cdot T$$
$$\hat{\mathbf{X}}(k+1) = \hat{\mathbf{X}}(k+1/k) + \delta\hat{\mathbf{X}}(k+1)$$
$$\delta\hat{\mathbf{X}}(k+1) = \mathbf{K}(k+1)\{\mathbf{Z}(k+1) - \mathbf{H}[\hat{\mathbf{X}}(k+1/k)]\}$$
$$\mathbf{P}(k+1/k) = \ddot{\mathbf{O}}(k+1/k)\mathbf{P}(k/k)\ddot{\mathbf{O}}(k+1/k)^T + \mathbf{Q}$$
$$\mathbf{K}(k+1) = \mathbf{P}(k+1/k)\mathbf{H}(k+1)^T[\mathbf{H}(k+1)\mathbf{P}(k+1/k)\mathbf{H}(k+1)^T + \mathbf{R}(k+1)]^{-1}$$
$$\mathbf{P}(k+1) = [\mathbf{I} - \mathbf{K}(k+1)\mathbf{H}(k+1)]\mathbf{P}(k+1/k)[\mathbf{I} - \mathbf{K}(k+1)\mathbf{H}(k+1)]^T + \mathbf{K}(k+1)\mathbf{R}(k+1)\mathbf{K}(k+1)^T$$

where $\mathbf{P}$ is the covariance matrix of the state estimation uncertainty, $\mathbf{K}$ is the Kalman gain matrix, $\ddot{\mathbf{O}}$ is the state transition matrix of the discrete dynamic system $\ddot{\mathbf{O}} \approx I + F \cdot T$, and T is the integration interval of the filter.

3. Simulation Overview

3.1 Simulation Description

A theoretical approach to the HEO determination has been described in the previous section. Here the proposed algorithm is implemented and its performance is analysed using a Monte-Carlo simulation[12]. The test scenario indicated in Figure 2 is used to analyse the performance of the proposed algorithm. It includes the following modules: GNSS satellite database, HEO satellite orbit dynamics, measurement computation and Kalman filter processing.

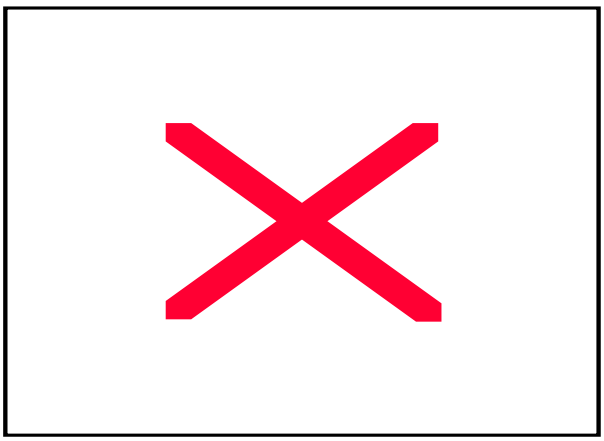

Figure 2: Orbit determination algorithm architecture.

Two HEO scenarios are chosen to test the algorithm. The scenario specifications are summarised in Table 1. HEO-1 is a geostationary transfer orbit with a low perigee, and an apogee close to the geostationary altitude. HEO-2 is a highly eccentric orbit. Figure 1 illustrates the relative size and shape of the two orbits.

Table 1. Selected HEO mission scenarios.

Parameter	HEO-1	HEO-2
Orbital Period (h)	10.5	23.5
Perigee Altitude (km)	349	12756
Apogee Altitude (km)	35800	57402
Semimajor Axis (km)	24446.0	41457.0
Eccentricity	0.7248	0.53846
Inclination (deg)	26.4	28.5
Argument of Perigee (deg)	137.0	0.0
Ascending Node (deg)	358.0	90.0
Mean Anomaly (deg)	0.0	0.0
Spacecraft Attitude	Three-axis stabilised, Earth-pointing	Three-axis stabilised, Earth-pointing

For these two scenarios, a single nadir-pointing GNSS antenna is assumed with the following antenna half-cone parameters:

- Navigation satellite transmit antenna half-cone angle: 21.3°[13] (The side lobe signals are generally lower power than signals transmitted form the main bean, since multi-GNSS is assumed , the simulation only considers receiving the main lobe.) .
- User satellite receiver antenna half-cone angle: 90° (main lobe) .

The Satellite Tool Kit (STK, v5.0) software (www.stk.com) is used to generate the satellite ephemerides to establish the GNSS Satellite Database. The initial almanac (i.e. osculating orbit parameters) of the GPS and GLONASS constellations was adopted from the web sources (**Table 2**). GNSS satellite orbits were generated using the actual broadcast ephemeris. Relevant parameters are listed in Table 3.

Table 2. Almanac sources.

Constellation	Sat Number	Almanac Source
GPS	31	http://www.glonass-ianc.rsa.ru
GLONASS	24	http://www.glonass-ianc.rsa.ru
GALILEO	30	http://www.esa.int/esaNA/galileo.html
COMPASS	35	See reference [14]
Total	120	

Table 3. GNSS measurement and error model simulation parameters.

Parameters	Value
Observation rate	1s
Elapsed hours	24 hours
GNSS constellation ephemerides	Broadcast from 30 April 2009 at 12:00:0 0.00 UTCG, to on 1 May 2009 at 12:00: 00 UTCG.
Visibility constraints	Earth blockage; Transmitting antenna beam width; Receiving antenna horizon masks.
Random pseudorange errors	5m

3.2 Signal Visibility

The test scenario assumes the GNSS receiver has a down-looking antenna to the Earth. The possible impact of the weak signal tracking is not discussed. Satellites are considered as visible and available if their line-of-sight is inside the transmission cone and the reception cone, and does not intersect with the Earth.

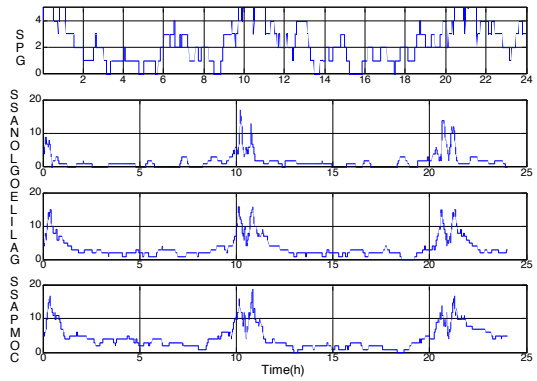

a) Single GNSS visibility conditions for HEO-1

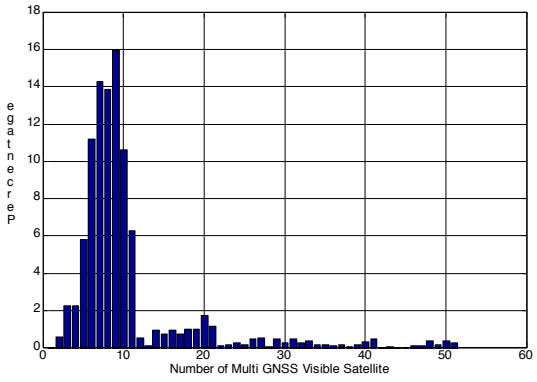

b) Percentage of N satellites tracked for HEO-1

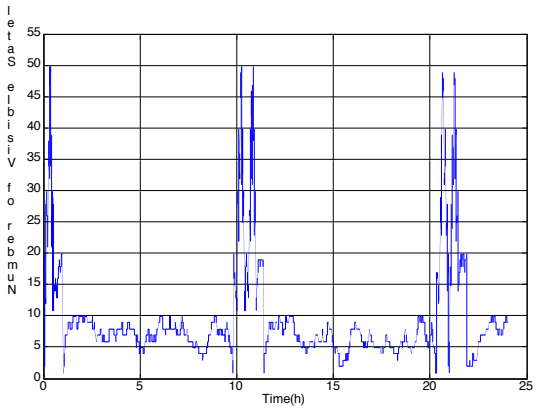

c) The multi-GNSS visibility conditions for HEO-1

Figure 3. HEO-1 tracking performance.

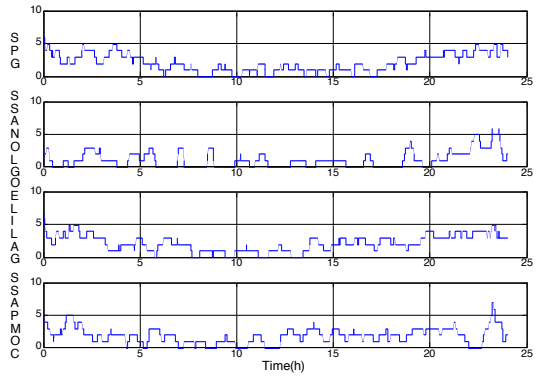

a) Single GNSS visibility conditions for HEO-2

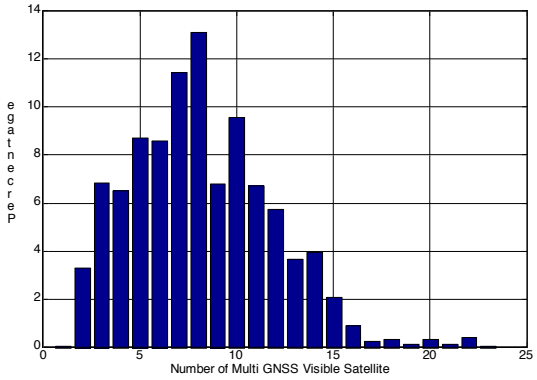

b) Percentage of N satellites tracked for HEO-2

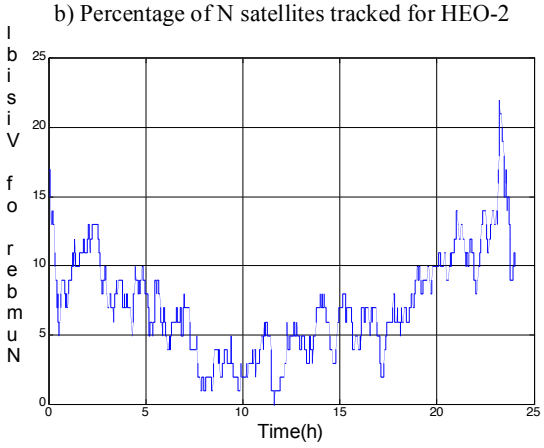

c) The multi-GNSS visibility conditions for HEO-2

Figure 4. HEO-2 tracking performance.

In a highly eccentric orbit in which altitude varies greatly, the best GNSS visibility can be obtained at the perigee and the worst at the apogee. This is evident in Figure 3 and 4. If multi-GNSS are used, 5 to 10 satellites are visible for more than 50% of the observation session.

3.3 Navigation Filtering Results

The assumed values for the covariance matrix of the process noise $\mathbf{W}(k)$ are:

$$\mathbf{Q}(k) = diag([(0.02\text{m})^2, (0.02\text{m})^2, (0.02\text{m})^2, (2\times10^{-4}\,\text{m/s})^2, (2\times10^{-4}\,\text{m/s})^2, (2\times10^{-4}\,\text{m/s})^2, (0.5m)^2, (1\times10^{-6}m)^2])$$

The initial errors of the satellite position and velocity are:

$$\delta\mathbf{X}(0) = [1000\text{m}, 1000\text{m}, 1000\text{m}, 1\text{m/s}, 1\text{m/s}, 1\text{m/s}, 300\text{m}, 0.0003\text{m}]$$

The initial covariance matrix of the satellite position and velocity is:

$$\mathbf{P}(0) = diag([(1000\text{m})^2, (1000\text{m})^2, (1000\text{m})^2, (1\text{m/s})^2, (1\text{m/s})^2, (1\text{m/s})^2, (300\text{m})^2, (0.0003\text{m})^2])$$

The errors of position and velocity are assumed to be:

$$\delta r = \sqrt{(\hat{x}-x)^2 + (\hat{y}-y)^2 + (\hat{z}-z)^2}$$

$$\delta v = \sqrt{(\hat{v}_x - v_x)^2 + (\hat{v}_y - v_y)^2 + (\hat{v}_z - v_z)^2}$$

where x, y, z, v_x, v_y, v_z are the true values of the satellite position and velocity, and $\hat{x}, \hat{y}, \hat{z}, \hat{v}_x, \hat{v}_y, \hat{v}_z$ are the estimated values. If the value of the position error δr is computed for N different samples $(\delta r_1, \delta r_2, \ldots \delta r_N)$, then the root mean square (RMS) of δr is defined as:

$$RMS(\delta r) = \sqrt{E(\delta r^2)} \cong \sqrt{\frac{1}{N}\sum_{i=1}^{N} \delta r_i^2}$$

The RMS of δv is:

$$RMS(\delta v) = \sqrt{E(\delta v^2)} \cong \sqrt{\frac{1}{N}\sum_{i=1}^{N} \delta v_i^2}$$

Orbit determination errors for the HEO-1 and HEO-2 scenarios are summarised in Table 4. The convergence of the Kalman filter for the HEO-1 and HEO-2 scenarios can be seen in Figure 5 and 6. As multi-GNSS provides redundant satellite signals, an accuracy of less than 100m (1σ) and 0.02m/s (1σ) is obtained for both test scenarios.

Table 4. Summary of orbit determination errors.

Scenario	HEO-1	HEO-2
RMS Position Error (m)	102.457	66.830
RMS Velocity Error (m/s)	0.021	0.022

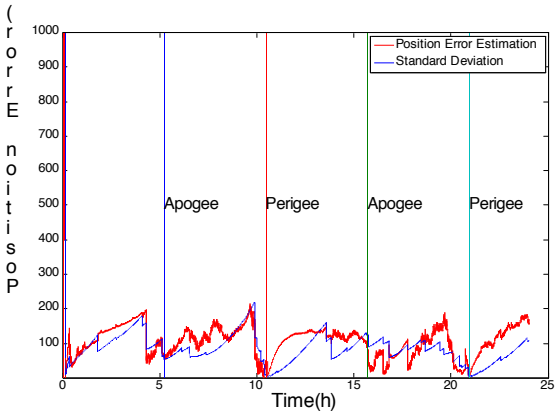

a) Ensemble RMS position errors

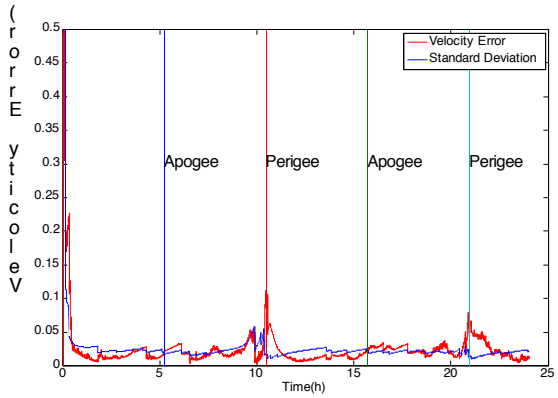

b) Ensemble RMS velocity errors

Figure 5. Convergence of Kalman filter (HEO-1).

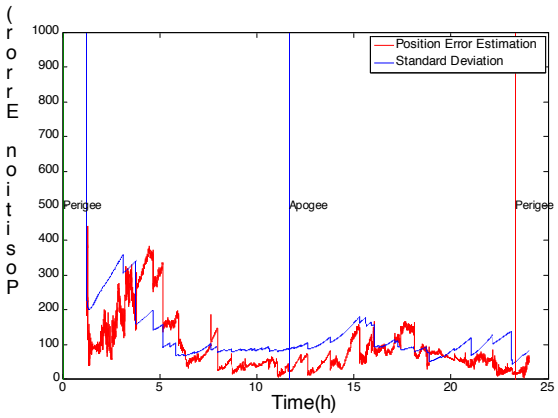

a) Ensemble RMS position errors

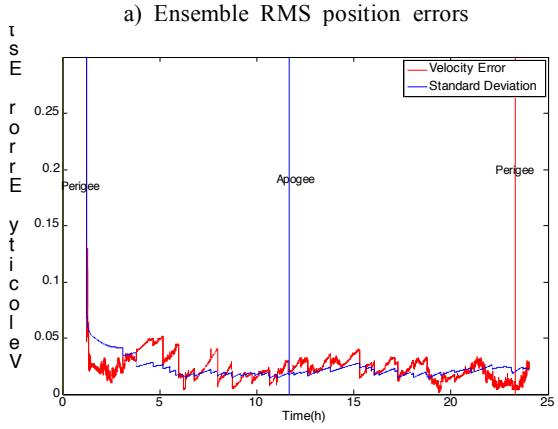

b) Ensemble RMS velocity errors

Figure 6. Convergence of Kalman filter (HEO-2).

4. Concluding Remarks

The application of multi-GNSS signals for precise HEO determination is not only possible but also practical, as demonstrated by the results of the simulation study presented in this paper. No single GNSS can solve the problem of HEO's line-of-sight non-availability, however, multi-GNSS provides a redundant number of visible satellites and therefore ensures an accurate orbit determination. In this study, the Extended Kalman filter is applied to multi-GNSS simulated observations in order to determine the orbit with an acceptable accuracy (< 200m 1σ for position vectors, and < 0.1m/s 1σ for velocity vectors).

Acknowledgement

The authors wish to thank their colleagues from the School of Surveying and Spatial Information Systems, University of New South Wales, Australia, and the College of Automation Engineering, Nanjing University of Aeronautics and Astronautics, P.R. China.

The first author wishes to thank the China Scholarship Council for the scholarship support during her joint training.

Reference

Moreau, M.C., Axelrad, P., Garrison, J.L., Long, A.C. (2000): GPS Receiver Architecture and Expected Performance for Autonomous Navigation in High Earth Orbits. *Navigation*, 47(3), 191-204.

Issler, J., Lestarquit, L., Grondin, M., Charmeau, M., Laurichesse, D., Lamy, A., Vincendet, C., Cazaux, C., Legrand, F., Benhallam, A. (1999): New Space GNSS Navigation Experiments. *12th Int. Tech. Meeting of the Satellite Division of the U.S. Inst. of Navigation*, Nashville, Tennessee, 14-17 September, page numbers???

Brodie, P.M., Doyle, L.J. (1999), *Technique for the Use of GPS for High Orbiting Satellites*. US Patent 5,935,196.

Haas, L., Pittelkau, M. (1999): Real-Time High Accuracy GPS Onboard Orbit Determination For Use On Remote Sensing. *12th Int. Tech. Meeting of the Satellite Division of the U.S. Inst. of Navigation*, Nashville, Tennessee, 14-17 September, 829-836.

Muellerschoen, R., Reichert, A., Kuang, D., Heflin, M., Bertiger, W., Bar-Sever, Y. (2001): Orbit Determination with NASA's High Accuracy Real-time Global Differential GPS System. *14th Int. Tech. Meeting of the Satellite Division of the U.S. Inst. of Navigation*, Salt Lake City, Utah, 11-14 September, page numbers????

Oliver., B., Eisfeller, B., Hein, G.W., Zink, T., Enderle, W., Schmidhuber, M., Lemke, N. (1998): Tracking GPS

Above GPS Satellite Altitude: Results of the GPS Experiment on the HEO Mission EQUATOR-S. *11th Int. Tech. Meeting of the Satellite Division of the U.S. Institute of Navigation*, Nashville, Tennessee, 15-18 September, page numbers???.

Moreau, M.C., Davis, E.P., Carpenter, J.R., Kelbel, D., Davis, G.W., Axelrad, P. (2002): Results from the GPS Flight Experiment on the High Earth Orbit AMSAT OSCAR-40 Spacecraft. *15th Int. Tech. Meeting of the Satellite Division of the U.S. Inst. of Navigation*, Portland, Oregan, 24-27 September, page numbers????.

Rizos, C. (2008): Multi-Constellation GNSS/RNSS From the Perspective of High Accuracy Users in Australia. *Journal of Spatial Sciences*, 53(2), 29-63.

Vallado, D.A., McClain, W.D. (2001): *Fundamentals of astrodynamics and applications*. Second ed. Boston , Space Technology Library, Kluwer Academic Publishers.

Montenbruck, O., Eberhard, G. (2000): *Satellite orbits: models, methods, and Applications*. First ed. Berlin, Springer Verlag.

Campana, R., Marradi, L. (2000): GPS-based Space Navigation: Comparison of Kalman Filtering Schemes. *13th Int. Tech. Meeting of the Satellite Division of the U.S. Inst. of Navigation*, Salt Lake City, Utah, 19-22 September, 1636-1645.

Minkler, G., Minkler, J. (1993): *Theory and Application of Kalman Filtering*. Magellan Book Company, Palm Bay, Florida, USA, 608pp.

Moreau, M.C., Axelrad, P., Garrison, J.L., Wennersten, M., Long, A.C. (2001): Test Results of the PiVoT Receiver in High Earth Orbits using a GSS GPS Simulator. *14th Int. Tech. Meeting of the Satellite Division of the U.S. Inst. of Navigation*, Salt Lake City, Utah, 11-14 September, 2316-2326.

Tan, S. (2008): Development and Thought of Compass Navigation Satellite System. *Journal of Astronautics*, 29(2), 391-396.